JTTEE5 19:586–601
DOI: 10.1007/s11666-009-9457-4
1059-9630/$19.00 © ASM International

Peer Reviewed

A Fitting Formula for Predicting Droplet Mean Diameter for Various Liquid in Effervescent Atomization Spray

Lijuan Qian, Jianzhong Lin, and Hongbin Xiong

(Submitted May 9, 2009; in revised form September 23, 2009)

The outflow of the effervescent atomization spray is simulated by a comprehensive numerical model based on the Navier-Stokes equation and the particle tracking method. The droplet mean diameter under different operating conditions and liquid properties were calculated. Based on the extensive computations, a formula relating droplet Sauter mean diameter to the operating conditions and liquid physical parameters were obtained with curve fitting technique. The results calculated from the formulae were compared with the experimental data and a good agreement was obtained. The formulae can be used to predict the droplet mean diameter for various Newtonian liquid in axisymmetric effervescent atomization spray conveniently and effectively.

Keywords effervescent atomization spray, fitting formula, liquid physical property, operating conditions

1. Introduction

Liquid atomization plays a pivotal role in a lot of engineering applications. As an essential step, the atomization is required to be controlled and efficient not only in traditional sprays such as spark ignition engines (Ref 1), soluble aqueous coatings (Ref 2, 3), but also in some novel approaches for thermal spray, for instance, suspension plasma spray (SPS) (Ref 4, 5) and solution-precursor plasma spray (SPPS) (Ref 6). However, the variety of operating conditions and atomizing liquid properties involving in these applications increase the difficulties in receiving stable finer atomization effects. A formula for the atomization properties as function of the operating conditions and liquid properties may be benefit to the engineering applications and experimental design.

Compared to other liquid atomization mechanisms, effervescent atomization, a method of twin-fluid process that involves bubbling gas into the liquid internally, has so far been found viable in many applications. The effervescent atomizer offers advantages of smaller drop sizes, reduced injection pressure, lower gas flow, lager exit orifice, higher viscosity over conventional pressure, rotary and twin-fluid atomizers. As summarized by Sovani et al.

Lijuan Qian and **Hongbin Xiong**, State Key Laboratory of Fluid Power Transmission and Control, Zhejiang University, Hangzhou 310027, P.R. China; and **Jianzhong Lin**, State Key Laboratory of Fluid Power Transmission and Control, Zhejiang University, Hangzhou 310027, P.R. China and China Jiliang University, Hangzhou 310018, P.R. China. Contact e-mails: qianlijuan1982@126.com and mecjzlin@public.zju.edu.cn.

Nomenclature

ALR	air-to-liquid ratio (by mass)
C_D	drag coefficient
D_{noz}	nozzle diameter (m)
d_l	droplet diameter (m)
e	internal energy (J)
F	force (N)
k, kk	dimensionless coefficient
$\dot{m}_l$	liquid mass flow rate ($kg \cdot s^{-1}$)
P_{in}	injection pressure ($kg \cdot m^{-1} s^2$)
Q	heat flux ($W \cdot m^{-2}$)
Re	Reynolds number (dimensionless)
sr	interface velocity slip ratio (dimensionless)
SMD	Sauter mean diameter (m)
SMD_0	initial SMD after primary breakup (m)
u, v, w	velocity (m/s)
V	volume
x	radial coordinate (m)
y	axial coordinate (m)

Greek symbols

α	volume fraction of gas
ζ	deformation parameter
μ	dynamic viscosity ($kg \cdot m^{-1} \cdot s^{-1}$)
ρ	density ($kg \cdot m^{-3}$)
σ	surface tension ($kg \cdot m^{-2}$)
ω	drop oscillation frequency (s^{-1})

Subscript

b	benchmark
cr	criteria
g	gas
l	liquid
o	orifice
p	particle

(Ref 7), the applications of effervescent atomization cover gas turbine combustors; IC engines; furnaces and boilers; incineration. In addition to these traditional applications, recently, Nislsen et al. (Ref 3) evaluated the actual potential of effervescent atomizer in atomization of high-viscosity aqueous solutions for coating applications. Esfarjani and Dolatabadi (Ref 5) simulated the internal liquid-gas flow in an effervescent nozzle for suspension plasma spray, modeling the suspension by considering the effect of nano-size particles on liquid phase as the change in the liquid bulk density and viscosity.

The effervescent atomization technique was developed in the late 1980s by Lefebvre and co-workers (Ref 8). During the past thirty years, abundant detailed experimental investigations concerning effervescent atomizer performance have been conducted (Ref 2, 3, 9-13), while the modeling studies are a few due to the high complexity of two-phase phenomena statistical behavior. In the aspect of modeling, Buckner and Sojka (Ref 14) developed a model to predict the mean droplet size from gas and liquid flow rates and liquid physical properties. Lund et al. (Ref 9) proposed a more fundamental model to predict droplet size from the atomizing gas and liquid mass flow rates, liquid physical properties, and atomizer exit geometry, without considering the aerodynamic effect of gas. Sutherland et al. (Ref 10) improved Lund's model, incorporating the effect of relative velocity between the atomizing gas and the liquid. All of these models are able to predict the droplet mean size after primary breakup, while without considering secondary atomization, these models cannot account for the spray evolution along the downstream of the exit orifice, which is critical to the engineering applications of atomization sprays. Xiong et al. (Ref 15) proposed a three-dimensional model to predict the droplet mean size and other spray characteristics by describing both primary and secondary atomization. Lin et al. (Ref 16) used Xiong et al.'s and an analytical model to simulate numerically the process of effervescent atomization impinging spray and deduced new formulae which relate deposition properties to the operating parameters. Nevertheless, the formulae did not take into account the effect of liquid physical properties on droplet mean size and only can be used for liquid water atomization. In most practical applications, however, the atomized liquids always span a wide range of physical properties. Therefore, it is necessary to improve the formulae (Ref 16) by incorporating the effects of liquid physical properties on droplet mean size.

In this study, firstly a comprehensive numerical model based on the Navier-Stokes equation and the particle tracking method is used to simulate numerically the effervescent atomization spray. The gas flow field is assumed to be axisymmetric and the dispersed droplets are modeled as Lagrangian entities. The evolutions of droplet mean size and the distributions of droplet number and size as well as the Weber number are analyzed. Then, based on extensive computations, a formula relating droplet mean diameter to operating conditions and liquid physical properties is deduced with curve fitting technique. Finally, data calculating from the formula of predicting droplet mean diameter are compared with numerical and available experimental results (Ref 5-7, 9-13) for fluids with various viscosities and surface tensions.

2. Mathematical Model

Figure 1 shows a schematic of the effervescent atomization impinging spray employed in this study. The entire process can be divided into three steps. The first step is the internal-mixing atomization in which atomizing gas is bubbled into the bulk liquid at low velocity and form bubbles, which produce a two-phase flow at the atomizer orifice. The experiments (Ref 7, 11) have indicated that an annular flow pattern at nozzle exit is beneficial for obtaining finer droplets. The second step takes place closed to the exit orifice. Leaving the nozzle exit, the rapidly expanding gas phase will shatter the squeezed liquid into fine droplets, which can be called as primary atomization. These droplets are unstable in the turbulent spray. In the third step, they will undergo a series of events such as collision, breakup and coalescent, which can be named as secondary breakup.

The present modeling work will focus on the external two-phase flow out of the effervescent atomizer exit. A comprehensive three-dimensional model involved primary breakup and secondary breakup is presented to predict the droplet diameter downstream of the nozzle exit. The Reynolds-averaged Navier-Stokes equations with k-ε models were used for gas phase, taking into account of two-way coupling of droplets and gas phase. Dispersed phase droplet is modeled as Lagrangian entities, accounting for the physical phenomena of droplet generation from primary and secondary breakup, droplet collision and coalescence, droplet momentum transfer.

2.1 Gas Phase Modeling

The external gas flow is turbulent, and the conservation equations for the mass, momentum, and energy for the gas are written in terms of vectors and tensors as follows:

$$\frac{\partial \rho}{\partial t} + \nabla \cdot (\rho \boldsymbol{u}) = 0, \quad \text{(Eq 1)}$$

$$\frac{\partial (\rho \boldsymbol{u})}{\partial t} + \nabla \cdot (\rho \boldsymbol{u}\boldsymbol{u}) = -\nabla \left(p + \frac{2}{3}\rho k \right) + \nabla \cdot [\sigma] + F, \quad \text{(Eq 2)}$$

$$\frac{\partial (\rho e)}{\partial t} + \nabla \cdot (\rho e \boldsymbol{u}) = -p \nabla \cdot \boldsymbol{u} - \nabla \cdot \boldsymbol{q} + \rho \varepsilon + Q, \quad \text{(Eq 3)}$$

where ρ is the gas density, $\boldsymbol{u}$ is the gas velocity vector, F is the momentum source or sink due to discrete liquid phase (grouped as computational parcels), k is the turbulent kinetic energy per unit mass, σ is the viscous shear stress tensor, $\boldsymbol{q}$ is the heat flux vector, ε is the viscous dissipation rate, and Q is the heat source or sink due to liquid droplets, e is the internal energy. The standard k-ε model is used to describe the turbulence effects. F and Q are used to couple the momentum and heat exchange from the liquid droplets to the gas phase. For this purpose, it is

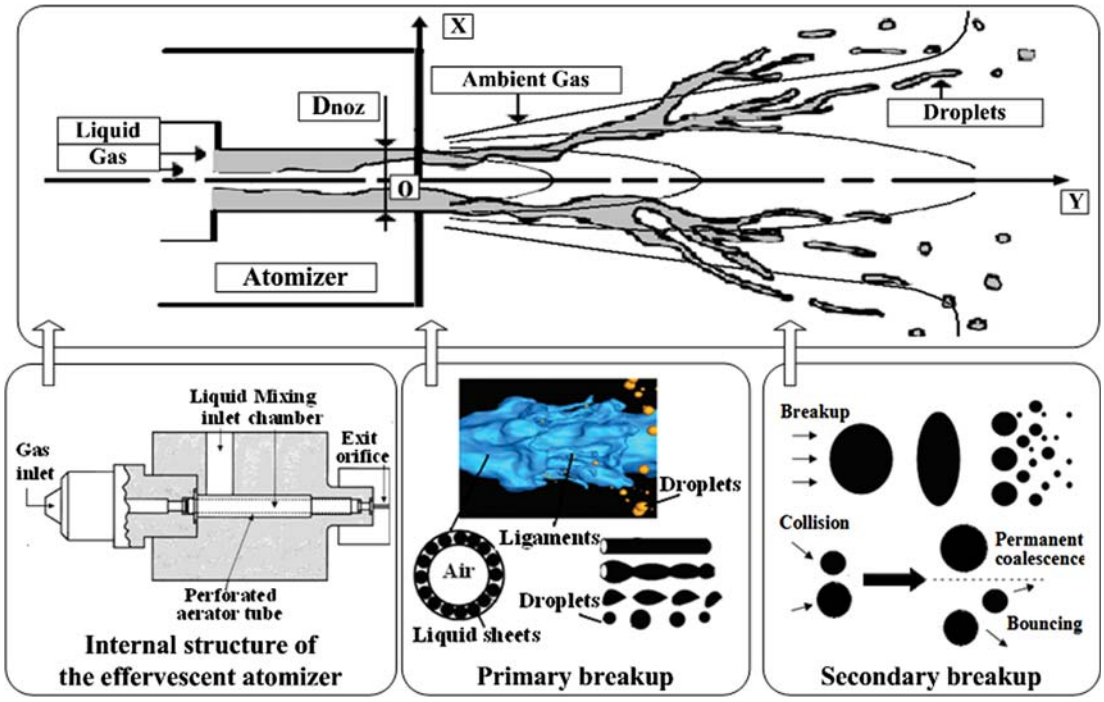

Fig. 1 Schematic of the effervescent atomization spray

necessary to sum over all particles in a computational cell. In each cell, the droplets are assumed to have the same parameters such as position, size, velocity, and temperature. Therefore, for a dilute spray, F and Q are defined as

$$F = -\frac{1}{V_{\text{cell}}}\sum_{P} N_{\text{p}} F_{\text{p}}, \qquad \text{(Eq 4)}$$

$$Q = \frac{1}{V_{\text{cell}}}\sum_{p} N_{\text{p}}\left[Q_{\text{p}} + F_{\text{p}}(u - v_{\text{p}})\right], \qquad \text{(Eq 5)}$$

where V_{cell} is the cell volume, N_{p} is the number of the droplets of this parcel, and F_{p} is the force acting on each droplet, Q_{p} is heat flux at each droplet surface, and v_{p} is the particle velocity.

2.2 Droplet Phase Modeling

The droplets parcels calculated are discretely treated in a Lagrangian manner. It is assumed that the droplets are added into the gas phase randomly from the annular sheath of the orifice exit uniformly across the nozzle exit. Multiple droplets have size, velocity, direction, and position distributions at injection. These initial droplet characteristics are provided by a one-dimensional primary breakup model combined with experimental distributions, which will be presented in detail in Sect. 3.

2.2.1 Sub-Model of Droplet Primary Breakup. Based on the experimental phenomena (Ref 7, 11), it is assumed that the two-phase flow pattern is regularly annular and the formed ligaments can be approximated by cylindrical jets (as Fig. 1 shows). Three sub-processes occur during primary breakup: first, the annular sheath liquid breaks into a number of cylindrical ligaments with almost the same diameter as the thickness of the annular sheet; secondly, the ligaments break into ligament fragments at the wavelength of the most rapidly growing wave; finally, the ligament fragments are stabilized to form one spheric droplet under the influence of surface tension.

In order to estimate annular liquid sheet thickness, it is assumed that the annular two-phase flow within the discharge orifice is one-dimensional, inviscid, and isothermal with compressible ideal gas and small interface velocity slip ratio. The momentum equation of the annular flow can then be written as the Bernoulli equation:

$$\frac{dp}{\rho_{\text{g}}} + v_{\text{g}} dv_{\text{g}} = 0, \qquad \text{(Eq 6)}$$

where p is the gas pressure, ρ_{g} is the gas density, v_{g} is the gas velocity. Combined with the state equation, Eq 6 can be integrated to

$$RT\ln(\rho_{\text{g}}\text{RT}) + \frac{1}{2}\left(\frac{\dot{m}_{\text{l}}\,\text{ALR}}{\rho_{\text{g}}\pi r_{\text{g}}^2}\right)^2 = \text{const} \qquad \text{(Eq 7)}$$

where r_{g} is the radius of gas flow, $\dot{m}_{\text{l}}$ the mass flow rate of liquid, and ALR is the air-liquid ratio by mass. The radius of gas flow can be written in terms of orifice radius r_{o} and void fraction α, $r_{\text{g}} = \sqrt{\alpha} r_{\text{o}}$. The interface velocity slip ratio r_{slip} under different flow rate is expressed as (Ref 17).

$$r_{\text{slip}} = \sqrt{\frac{\rho_{\text{l}}}{\rho_{\text{g}}}\frac{\sqrt{\alpha}}{1 + C(1-\alpha)}}, \qquad \text{(Eq 8)}$$

This slip ratio correlation is originally proposed by Ishii (Ref 18) and applicable for two-phase annular flow. In Eq 8, C is the experimental coefficient, which is close to 1 in the present study. The relations between the interface velocity slip ratio and void fraction are proposed by Todreas and Kazimi (Ref 19) and expressed as:

$$1+\frac{\rho_g sr}{\rho_l \mathrm{ALR}}=\frac{1}{\alpha}. \qquad \text{(Eq 9)}$$

By solving Eq 7-9, ρ_g, α and r_{slip} can be calculated for different operating conditions. The thickness of annular liquid sheet is then calculated from $\delta = r_o - r_g$, which is also the diameter of the typical cylindrical ligament.

The breakup wave length λ is determined by the wave number k_ω at which value the maximum growth rate ϑ occurs. The growth rate of surface disturbances ϑ is estimated by Senecal et al. (Ref 20) solutions, as follows:

$$\vartheta=-\frac{2\mu_l k_\omega^2 \tanh(k_\omega h)}{\tanh(k_\omega h)+\rho^*}+\frac{\sqrt{4\mu_l^2 k_\omega^4 \tanh^2(k_\omega h)-\rho^{*2} v_s^2 k_\omega^2-[\tanh(k_\omega h)+\rho^*]\left(-\rho^* v_s^2 k_\omega^2+\sigma_l k_\omega^3/\rho_l\right)}}{\tanh(k_\omega h)+\rho^*} \qquad \text{(Eq 10)}$$

where k_ω is the wave number given by $k_\omega = 2\pi/\lambda$, h is the half-thickness of sheet $h = \delta/2$, $\rho^* = \rho_g/\rho_l$ is the gas/liquid density ratio, v_s is the liquid sheet velocity. Here, the value of the liquid sheet velocity is assumed to be the same as the relative velocity difference of the gas and the liquid at the nozzle exit. Assuming that each fragment is stabilized to one droplet, the Sauter mean drop diameter SMD (defined as the ratio of volume-to-surface area) can then be calculated from the conservation of mass:

$$\mathrm{SMD}=\left[\frac{3}{2}\delta^3\lambda\right]^{1/3}, \qquad \text{(Eq 11)}$$

2.2.2 Sub-Model of Droplet Secondary Breakup. As Fig. 1 shows, the sub-model of droplet secondary breakup includes droplet tracking, cascade atomization and droplet collision and coalescence.

2.3 Droplet Tracking

The liquid droplets are discretely treated in a Lagrangian manner. Computational droplets are generated at the points of injection and tracked throughout their flight. Assume that only drag force and gravity affect the droplet momentum transfer significantly for the droplet with size smaller than 100 μm, the momentum transfer between the droplet and atomization jet can be described by

$$F_p = m_p\frac{dv_p}{dt}=\frac{\pi r_p^2 \rho_l C_D}{2}|u-v_p|(u-v_p)+g, \qquad \text{(Eq 12)}$$

$$\frac{dx_p}{dt}=v_p, \qquad \text{(Eq 13)}$$

where m_p is the particle mass, g is the gravity force, and the coefficient of the drag force C_D can be expressed as

$$C_D = 24Re_p^{-1}+6\left(1+Re_p^{-1/2}\right)+0.4, \quad \text{for } Re_p = 2\rho r_p|u-v_p|/\mu<100. \qquad \text{(Eq 14)}$$

2.4 Cascade Atomization Modeling

To model the droplet secondary breakup, a cascade atomization and drop breakup model (Ref 21) has been utilized. The drop distortion is described by a forced, damped, harmonic oscillator in which the forcing term is given by the aerodynamic droplet/gas interaction, the damping is due to the liquid viscosity, and the restoring force is supplied by the surface tension.

The drop distortion is described by the deformation parameter, $\zeta = 2\tau/r$, where τ denotes the change of radial

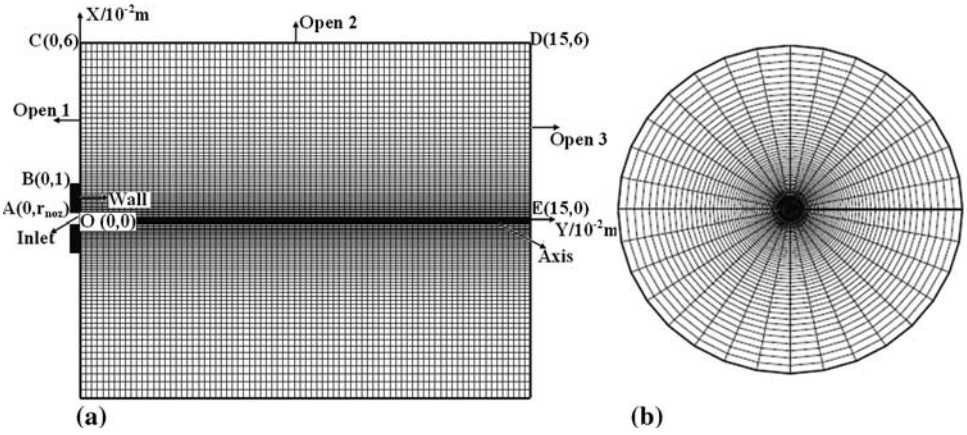

Fig. 2 Geometry and computational mesh: (a) middle section plane and (b) cross-sectional plane in radial and azimuthal directions

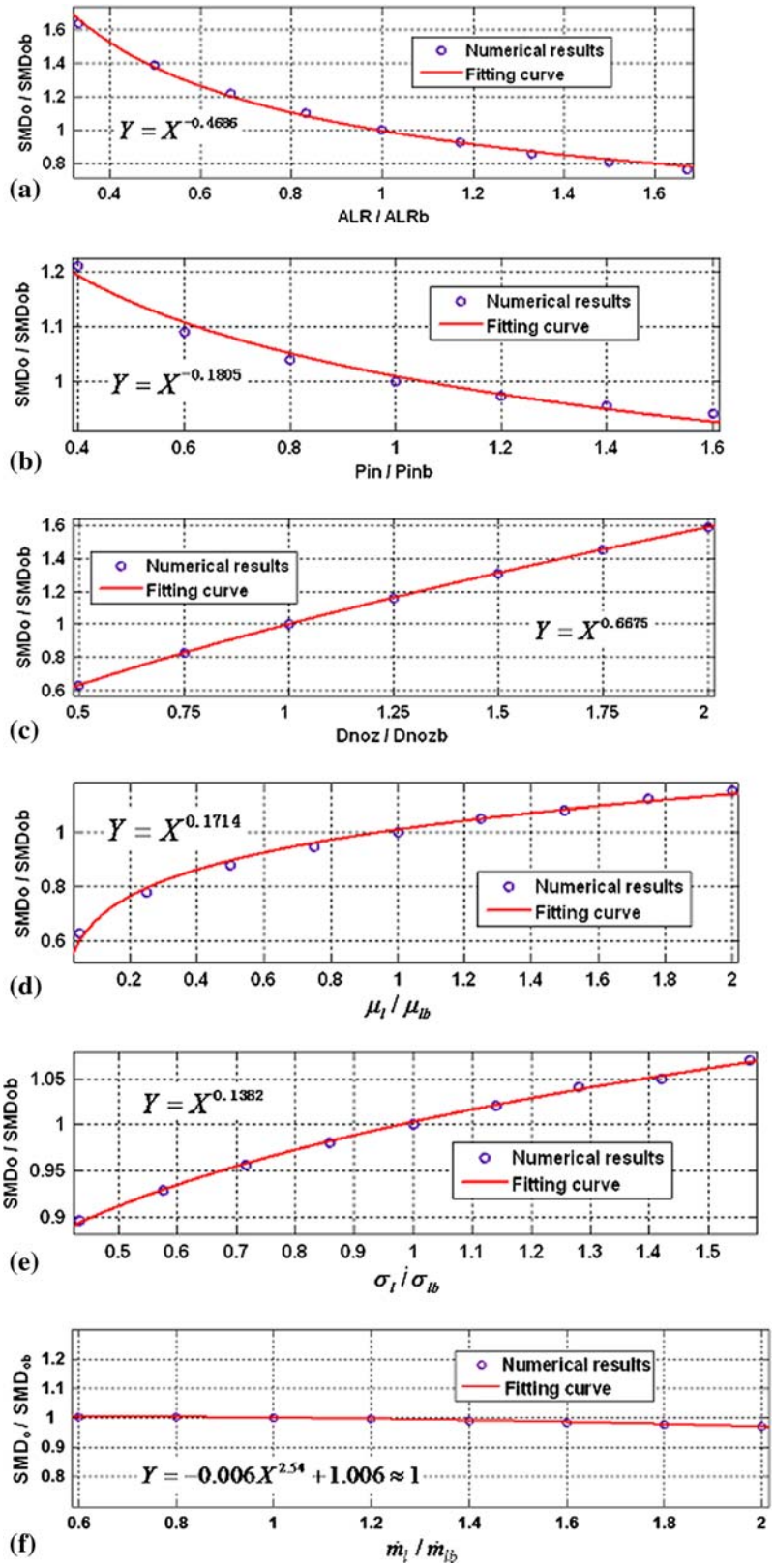

Fig. 3 Relationships between SMD_0 and independent parameters. (a) $SMD_0 \sim$ ALR, (b) $SMD_0 \sim P_{in}$, (c) $SMD_0 \sim D_{noz}$, (d) $SMD_0 \sim \mu_l$, (e) $SMD_0 \sim \sigma_l$, and (f) $SMD_0 \sim \dot{m}_l$

cross-section from its equilibrium position and r is the drop radius. The deformation equation of ζ in terms of the normalized distortion parameter is

$$\ddot{\zeta} + \frac{5\mu_l}{\rho_l a^2}\dot{\zeta} + \frac{8\sigma}{\rho_l a^3}\zeta = \frac{2\rho_g |U|^2}{3\rho_l a^2}, \quad \text{(Eq 15)}$$

where ρ is the density, μ is the viscosity, σ is the surface tension, U is the relative drop-gas velocity, and the subscripts g and l denote the gas or liquid, respectively. Drop breakup occurs when the normalized drop distortion, $\zeta(t)$, exceeds the critical value of 1.

The creation of the product droplets is derived using elements from population dynamics, i.e., for each breakup event it is assumed that the number of product droplets is proportional to the number of critical parent drops, where the proportionality constant depends on the drop breakup regime. From this, we can define the rate of droplet creation, which, in conjunction with the mass conservation principle between parent and product droplets, leads to the basic cascade breakup law:

$$\frac{d}{dt}\bar{m}(t) = -3K_{bu}\bar{m}(t), \quad \text{(Eq 16)}$$

where $\bar{m}(t)$ denotes the mean mass of the product drop distribution, and the breakup frequency K_{bu} depends on the drop breakup regimes. As suggested by Reitz (Ref 22), three breakup regimes are classified with respect to increasing the gas Weber number into bag breakup, stripping breakup regime, and catastrophic breakup regime. While in this study, the gas Weber number is mostly lower than 80, which falls into bag breakup regime. Breakup frequency $K_{bu} = 0.05\omega$ as suggested by O'Rourke and Amsden (Ref 23) is used here, and the drop oscillation frequency ω is given by

$$\omega^2 = \frac{8\sigma}{\rho_l a^3} - \frac{25\mu_l^2}{4\rho_l^2 a^4}. \quad \text{(Eq 17)}$$

Note that except for the mean mass $\bar{m}(t)$, the actual size distribution of the product droplet has not been specified yet. For the model implementation in this study, a uniform product drop size distribution has been assumed, by which Eq 16 becomes:

$$\frac{r}{a} = e^{-K_{bu}t_{bu}}, \quad \text{(Eq 18)}$$

where a and r are the radii of the parent and product drops, respectively, and t_{bu} is the breakup time, i.e., the time until the normalized deformation $\zeta(t)$in the solution of Eq 15 exceeds the value of 1.

2.5 Droplet Collision Modeling

The droplet collision and possible coalescence are modeled by a collision Weber number. Collisions between drops can result in bouncing, permanent coalescence, or coalescence followed by separation.

Most studies begin with defining the collision parameters which include collision Weber number, We_l, and impact parameter, $\psi = \chi/(r_1 + r_2)$, where χ is the distance between the center of one drop and the relative velocity vector u_r, r_1 and r_2 are the radii of small and large droplets, respectively. Two drops are considered to collide if they touch, and collision is treated as an instantaneous event. One drop replaces two colliding drops in a coalescence event, while bouncing drops simply change velocity. Separation-type collisions result is not considered in this study for the low relative velocity of drops.

The balance between surface, kinetic, and internal energy determines the collision regime. Coalescence occurs when surface energy dominates, while bouncing occurs when kinetic energy dominates. The criteria, χ_{cr}, determine the transition boundary between various regimes: drops coalescence when $\chi \le \chi_{cr}$, and bounces when $\chi > \chi_{cr}$. χ_{cr} can be expressed as

$$\chi_{cr}^2 = (r_1 + r_2)^2 \min\left[1.0, 2.4\frac{f(\gamma)}{We_l}\right] \quad \text{(Eq 19)}$$

where $We_l = \rho|U|r_1/\sigma(\bar{T}_d)$, ρ is the droplet density, $\sigma(\bar{T}_d)$ is the surface tension at average temperature of $\bar{T}_d$ in the following expression:

$$\bar{T} = \frac{r_1^3 T_1 + r_2^3 T_2}{r_1^3 + r_2^3} \quad \text{(Eq 20)}$$

where T_1 and T_2 are the temperature of the two colliding droplets, $f(\gamma)$ is a function of the radius ratio γ (Ref 23):

$$f(\gamma) = \gamma^2 - 2.4\gamma^2 + 2.7\gamma \quad (\gamma = r_2/r_1 \ge 1) \quad \text{(Eq 21)}$$

3. Computational Issues and Boundary Conditions

3.1 Computational Issues

Figure 2 shows the computational mesh with the size of 56 (radial) × 65 (axial) × 32 (azimuthal) in the cylindrical coordinate system. Finer meshes are used for the core region of the spray. The radius and axial lengths of the computational regime are 0.06 and 0.15 m, respectively, and 2π in the circular direction.

For the droplets, the initial size assigned to each particle is assumed as the mean diameter from primary breakup model with Rosin-Rammler distribution, which can be presented as: $F_{R-R}(D) = 1 - \exp\{-(D/\mathrm{SMD}_0)^q\}$, where q with the value of 5 in the present paper indicates the value of the width of the distribution (Ref 24). The initial droplet velocity is the mean droplet velocity from primary breakup model with a random deviation within 5%; the direction with regard to injector axis is given by a random distribution from 0 to the cone angle of 15°; the droplet positions are randomly distributed in the exit plane of the annular liquid sheath. A total number of 10,000 computational droplets are injected into the flow for each case.

3.2 Boundary Conditions

As shown in Fig. 2, there are five types of boundary conditions involved in three-dimensional simulation.

1. Three open boundaries are taken as either inward or outward flow conditions: Open 1 (line BC), where the pressure and temperature and axial velocity u are assigned the same as that in ambient if the mass flow is inward as $v(x,0,\theta)>0$, otherwise $\partial u/\partial y=0$ and $\partial\phi/\partial y=0$ is applied in which ϕ represents the temperature and pressure. Open 2 (line CD), ambient condition is used for $u(6,y,\theta)<0$, while $\partial\phi/\partial x=0$, $\partial v/\partial y=0$ for $u(6,y,\theta)>0$. Open 3 (line DE), the ambient condition is used for $v(x,15,\theta)<0$, while $\partial\phi/\partial y=0$ is used for $v(x,15,\theta)>0$.
2. Wall boundary at line AB: the velocity is zero and the temperature is set as 300 K; the turbulent wall function treatment is employed to calculate turbulent kinetic energy and viscous dissipation.
3. Inlet boundary is taken at the atomizer orifice (line OA), the condition of gas and droplets are calculated from the primary breakup model.
4. Axis boundary (at the axis $x=0$): the boundary condition which can include the non-axisymmetric effects in three-dimensional model is specified as $\xi|_{x=0}=\left(\sum_{i=1}^{N}\xi_i\right)/N(\xi=u,v,T)$ and the circular velocity $w=0$, where ξ_i are the values of ξ at location with the distance Δx from the centerline.
5. At the circular direction $\theta=2\pi$, periodic boundary is used.

4. Expression of Droplet Mean Diameter

The main task in the present study is to qualify the relationships between droplet mean diameter and liquid properties as well as the operating conditions. The droplet mean diameter will be reported in terms of Sauter mean diameter (SMD or d_{32}), which is defined as the ratio of volume-to-surface area.

For effervescent atomization sprays, abundant experimental results (Ref 11-13) and numerical simulations (Ref 15, 16) indicated that the evolution of the droplet SMD with the axial distance presented similar trends in various cases for different operating condition and liquid properties. The droplet diameter first decreases and then increases with the axial distance, the nadir of the curve resides approximately 1 cm downstream of the nozzle exit. (Computational validation will be presented in Sect. 5.1). This phenomenon results in a serious droplet transfer processes involved in atomization sprays and different droplet transfer mechanisms dominate in different ranges. First, closed to the exit orifice, the liquid sheets are atomized into small droplets. The initial droplet size SMD_0 can be determined by the primary atomization model (Sect. 2.2.1). Then, the secondary atomization dominated for a short distance within 1 cm from the atomizer exit leads to a decrease in droplet size. While further downstream, droplet coalescence dominates and results in an increase in droplet size. Supposed droplet mean size increases with the axial distance linearly, the relationship between SMD and the axial distance from nozzle exit y can be expressed as $SMD=k\times y+kk$, where k and kk are the coefficients identified by operating parameters and liquid properties. After obtaining SMD_0, k, kk, the values of SMD at $y\to 0$ and $y\approx 1$ cm will be known. If simplifying the changes of SMD between $y=0$ and $y=1$ cm to be linear, the general evolution of SMD along the axial distance can be expressed as:

$$\mathrm{SMD}=\begin{cases}\mathrm{SMD}_0 & y\to 0\\ (k+kk-\mathrm{SMD}_0)\times y+\mathrm{SMD}_0 & 0<y<1\text{ cm}\\ k\times y+kk & 1\text{ cm}\le y\le 20\text{ cm}\end{cases}, \quad \text{(Eq 22)}$$

where $y\le 20$ cm is given on the basis of most experimental (Ref 11-13) and simulation area (Ref 15, 16).

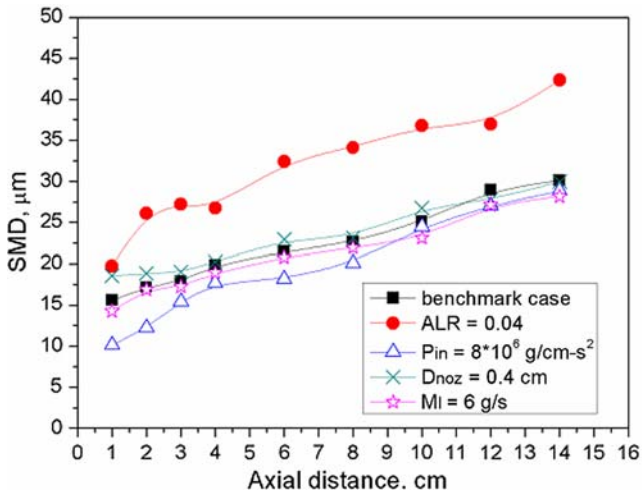

Fig. 4 Droplet SMD along axial direction under different conditions

Table 1 Parameters for the prediction of SMD_0 and SMD

Independent parameter	Air-to-liquid ratio (ALR)	Injection pressure, P_{in}, g/cm · s^2	Nozzle diameter, D_{noz}, cm	Liquid mass flow rate $\dot{m}_l$, g/s	Viscosity, μ, g/cm · s	Surface tension, σ_l, g/s^2
Range	0.04-0.2	2×10^6-8×10^6	0.05-0.4	6-20	0.01-0.4	20-72
Benchmark	0.12	5×10^6	0.2	10	0.2	46

Therefore, in order to predict the droplet mean diameter at different axial distance, the key step is to establish the expressions of k, kk and SMD_0 as the functions of operating conditions and liquid physical properties. A curve fitting method will be used upon extensive numerical computations. For concise writing, the CGS unit system is used below instead of SI units.

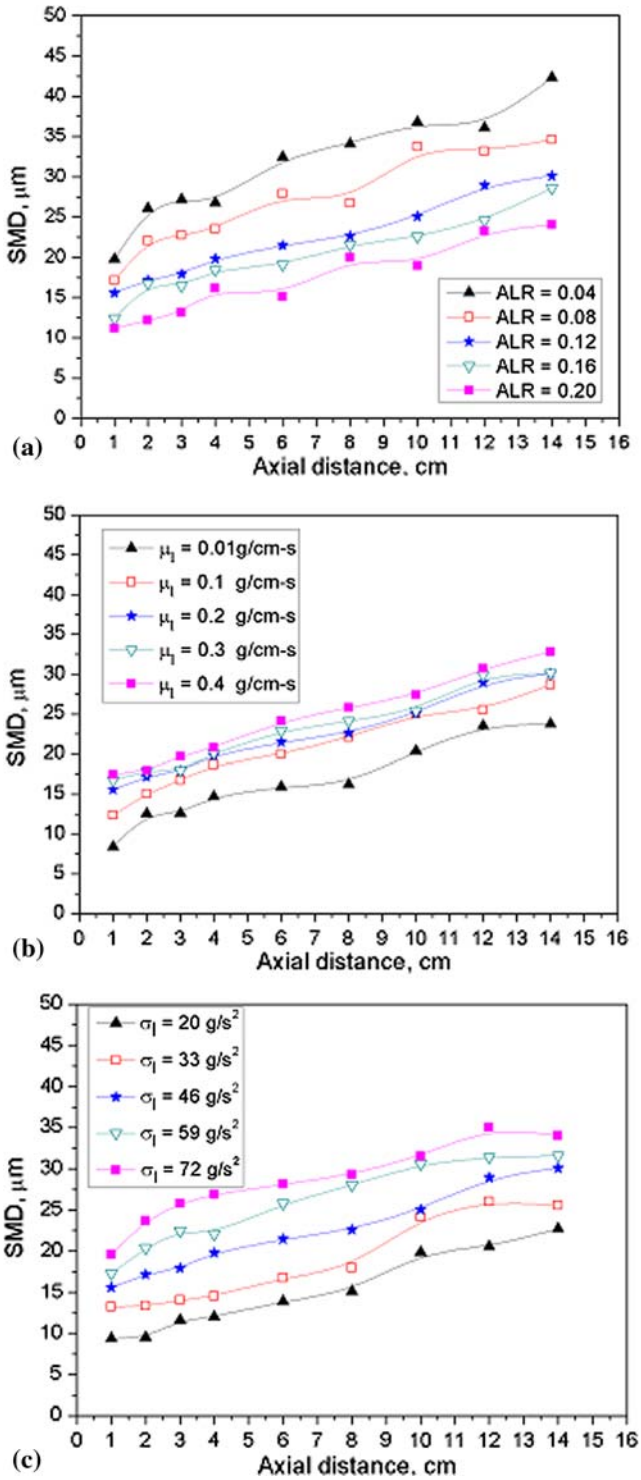

Fig. 5 Numerical results of SMD at different axial distance. (a) With different air-to-liquid ratio, (b) with different liquid viscosity, and (c) with different liquid surface tension

4.1 Expression of SMD_0

The factors that influence droplet mean diameter in an effervescent atomization cover a wide range. In the present study, only the leading factors are taken into consideration. As summarized by Sovani et al. (Ref 7), the main effective operating parameters are air-to-liquid mass ratio ALR, injection pressure P_{in}, atomizer orifice diameter D_{noz}. Liquid mass flow rate $\dot{m}_l$ is also an important operating parameter, especially for droplet velocity; however, the effect of liquid mass flow rate on droplet mean diameter is not obvious, as indicated by both experiments (Ref 11) and simulation results (Fig. 3f). The dominating liquid physical properties in atomization are surface tension σ_l and viscosity μ_l, while the influence of liquid density is minor.

Due to the complex correlations between SMD_0 and the operating parameters as well as liquid properties, the expression of SMD_0 is obtained with curve fitting technique. For the application of spray coating engineering (Ref 25) and most experimental conditions (Ref 7) indicated, the ranges of these independent parameters can be set as Table 1 shows. Then, the benchmarks used to normalize the data are obtained as $ALR_b = 0.12$, $P_{inb} = 5 \times 10^6$ g/cm · s^2, $D_{nozb} = 0.2$ cm, $\mu_{lb} = 0.2$ g/cm · s, $\sigma_{lb} = 46$ g/s^2, $\dot{m}_{lb} = 10$ g/s, and $SMD_{0b} = 0.00505$ cm.

Figure 3 shows the relationships between SMD_0 and the independent parameters, in which the subscript b means benchmark and all simulation results are calculated

Table 2 Variables related in SMD fitting technique

(a) With various ALR					
ALR	0.04	0.08	0.12	0.16	0.20
k	1.363	1.203	1.103	1.019	0.944
kk	22.35	18.09	14.72	13.05	11.57
SMD_0, μm	82.76	61.51	50.46	43.41	38.55
(b) With various liquid viscosity					
μ_l , g/cm · s	0.01	0.1	0.2	0.3	0.4
k	1.1	1.143	1.103	1.082	1.198
kk	9.118	12.82	14.72	15.57	16.09
SMD_0, μm	31.89	44.26	50.46	54.69	57.99
(c) With various liquid surface tension					
σ_l, g/s^2	20	33	46	59	72
k	1.065	1.132	1.103	1.101	1.023
kk	7.849	10.85	14.72	18.17	21.4
SMD_0, μm	45.21	48.24	50.46	52.24	53.76

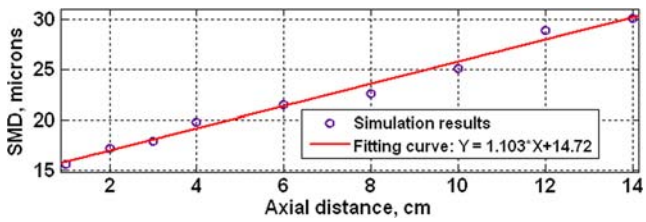

Fig. 6 Fitting curve of SMD vs. axial distance from the nozzle exit at ALR = 0.12, $\mu_l = 0.2$ g/cm · s, $\sigma_l = 46$ g/s^2

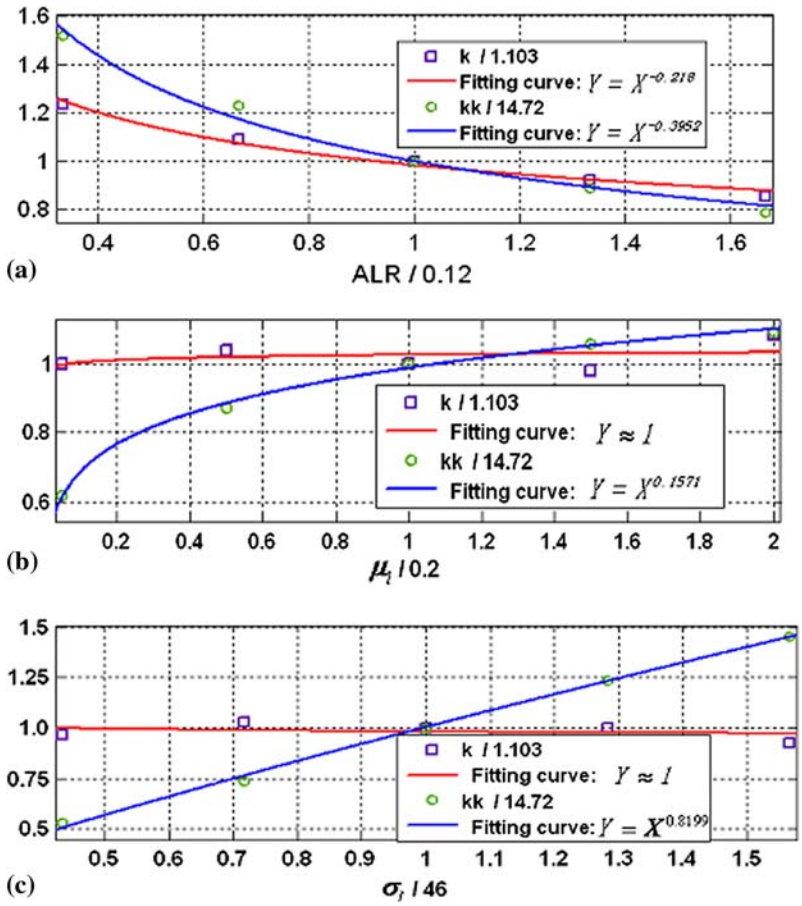

Fig. 7 Fitting curves of *k* and *kk*. (a) With various air-to-liquid ratio, (b) with various liquid viscosity, and (c) with various liquid surface tension

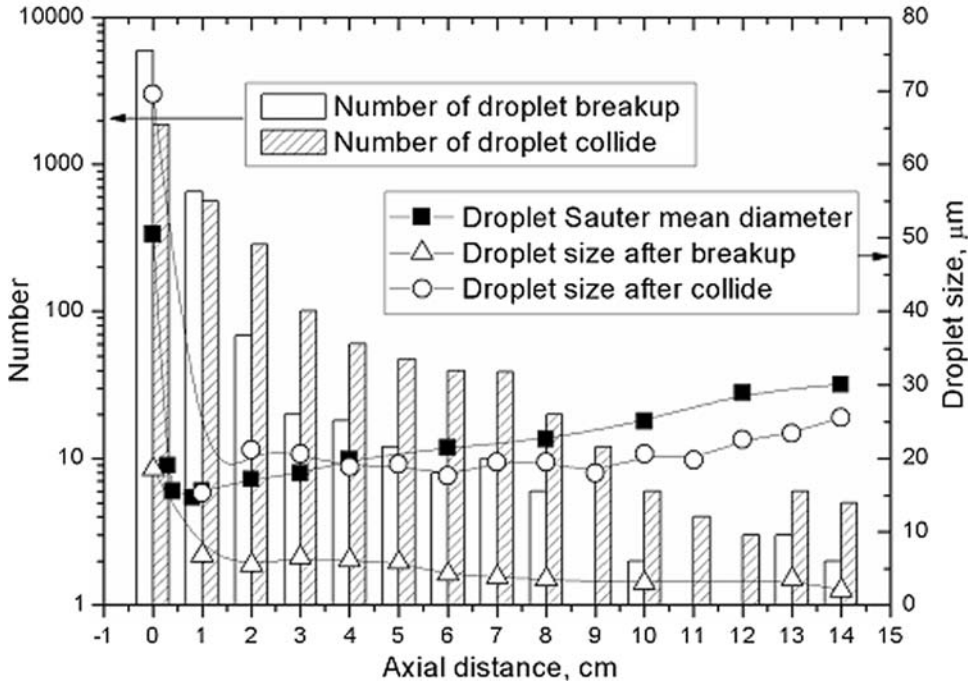

Fig. 8 Occurrence numbers of droplet collision and secondary breakup and the resulting droplet diameters

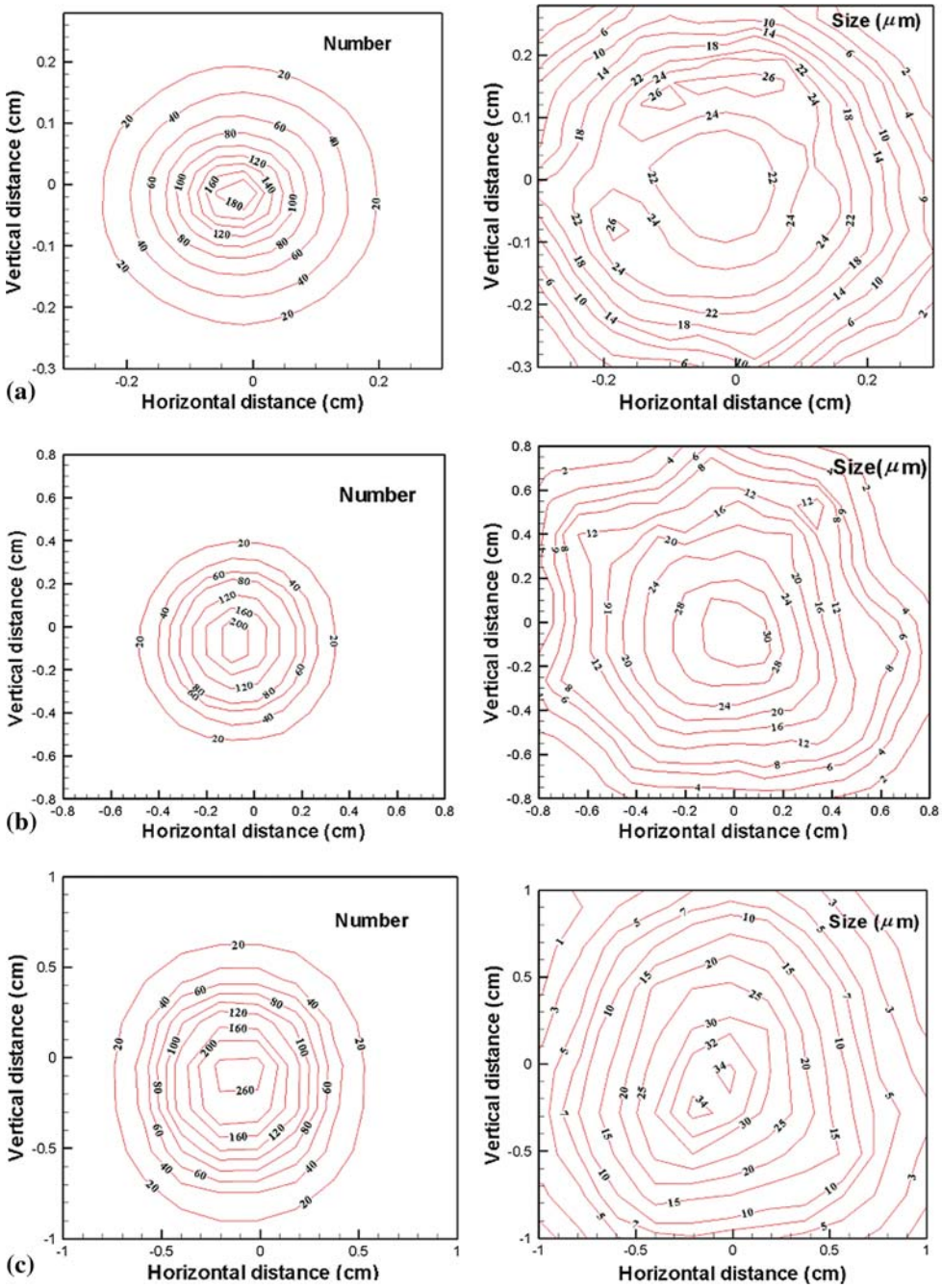

Fig. 9 Droplet size and number distribution at different cross-sectional plane. Axial distance = 50 mm (a), 100 mm (b), and 150 mm (c)

from the primary breakup model. It can be seen from Fig. 3(a) and (b), SMD_0 gradually decrease with the exponents of −0.4686 and −0.1805 as the ALR and P_{in} increase. The fitting curve can be expressed as $Y = X^{-0.4686}$, $Y = X^{-0.1805}$, respectively. While in Fig. 3(c)-(e), SMD_0 gradually increase with the exponents of 0.6675, 0.1382, 0.1714 as D_{noz}, μ_l, σ_l increase. The fitting equations are $Y = X^{0.6675}$, $Y = X^{0.1714}$, $Y = X^{0.1382}$, respectively. Figure 3(f) shows that the influence of $\dot{m}_l$ on SMD_0 is minor when ALR remains unchanged and the fitting expression can be approximated to $Y = 1$. By multiplying all the impacting factors in the form of dimensionless, SMD_0 can be expressed as:

$$\frac{SMD_0}{0.00505} = \left(\frac{ALR}{0.12}\right)^{-0.4686} \times \left(\frac{P_{in}}{5 \times 10^6}\right)^{-0.1805} \times \left(\frac{D_{noz}}{0.2}\right)^{0.6675} \times \left(\frac{\mu_l}{0.2}\right)^{0.1714} \times \left(\frac{\sigma_l}{46}\right)^{0.1382}, \quad \text{(Eq 23)}$$

where the unit system is CGS. From the exponents, the impact of each parameter on droplet initial mean size SMD_0 can be quantized.

4.2 Expression of $k \times y + kk$

Figure 4 analyzes the relative effect of operating parameters to the droplet mean diameter. All the cases have the same operating conditions as the benchmark case, except for the specified conditions in the legend. It can be seen from Fig. 4 that compared to ALR, the effect of other operating parameters like liquid mass flow rate, nozzle diameter, and injection pressure on the SMD is not significant at the downstream location away from the nozzle exit. Therefore, ALR is the main effective operating parameter that will be taken into consideration here.

The influences of ALR, liquid viscosity and surface tension on SMD with the axial distance of 1-14 cm, which is calculated from numerical simulations, are shown in Fig. 5. All the data in Fig. 5 are under the benchmark conditions (as Table 1 shows), with only one independent parameter varying between the ranges. In order to establish the relationships between $k \times y + kk$ and operating conditions as well as the liquid physical properties, a fitting technique is used. Firstly, as listed in Table 2, all the parameters of k and kk for each case in Fig. 5 are derived by the linear polynomial fitting technique, since SMD is almost proportional to the axial distance y. Taking the benchmark case as an example, Fig. 6 shows the fitting curve is $Y = k \cdot X + kk = 1.103 \cdot X + 14.72$. Secondly, ALR, μ_l, σ_l, k, kk in Table 2 are normalized by the benchmarks of 0.12, 0.2 g/cm s, 46 g/s^2, 1.103 and 14.72, respectively. The exponential fitting technique is used to relate k and kk to ALR, liquid viscosity and surface tension. As shown in Fig. 7(a), k and kk gradually decrease with the exponents of -0.218 and -0.3952 accordingly as the ALR increasing. The fitting curve is expressed as $Y = X^{-0.218}$ and $Y = X^{-0.3952}$, respectively. In Fig. 7(b) and (c), k is insensitive to the changes of liquid viscosity and surface tension. The fitting equations is $Y = 1$, while kk obviously raises with the exponents of 0.1571 and 0.8199 as liquid viscosity and surface tension increasing. The fitting formulas are $Y = X^{0.1571}$ and $Y = X^{0.8199}$, respectively. Finally, the expression of $k \times y + kk$ can be presented as:

$$k \times y + kk = 1.103 \times (\mathrm{ALR}/0.12)^{-0.218} \times 10^{-4} \times y + 14.72 \times (\mathrm{ALR}/0.12)^{-0.3952} \times (\mu_l/0.2)^{0.1571} \times (\sigma_l/46)^{0.8199} \times 10^{-4} \quad \text{(Eq 24)}$$

4.3 Expression of SMD

Based on the above analysis, Eq 22 can be rewritten by consisting of Eq 23 and 24:

$$\mathrm{SMD} \begin{cases} = 0.00505 \times \left(\frac{\mathrm{ALR}}{0.12}\right)^{-0.4686} \times \left(\frac{P_{in}}{5\times10^6}\right)^{-0.1805} \times \left(\frac{D_{noz}}{0.2}\right)^{0.6675} \times \left(\frac{\mu_l}{0.2}\right)^{0.1714} \times \left(\frac{\sigma_l}{46}\right)^{0.1382} & y \to 0 \\ = \left(1.103 \times \left(\frac{\mathrm{ALR}}{0.12}\right)^{-0.218} + 14.72 \times \left(\frac{\mathrm{ALR}}{0.12}\right)^{-0.3952} \times \left(\frac{\mu_l}{0.2}\right)^{0.1571} \times \left(\frac{\sigma_l}{46}\right)^{0.8199}\right) \times 10^{-4} \times y & \\ \quad + (1-y) \times 0.00505 \times \left(\frac{\mathrm{ALR}}{0.12}\right)^{-0.4686} \times \left(\frac{P_{in}}{5\times10^6}\right)^{-0.1805} \times \left(\frac{D_{noz}}{0.2}\right)^{0.6675} \times \left(\frac{\mu_l}{0.2}\right)^{0.1714} \times \left(\frac{\sigma_l}{46}\right)^{0.1382} & 0 < y < 1 \text{ cm} \\ = 1.103 \times \left(\frac{\mathrm{ALR}}{0.12}\right)^{-0.218} \times 10^{-4} \times y + 14.72 \times \left(\frac{\mathrm{ALR}}{0.12}\right)^{-0.3952} \times \left(\frac{\mu_l}{0.2}\right)^{0.1571} \times \left(\frac{\sigma_l}{46}\right)^{0.8199} \times 10^{-4} & 1 \text{ cm} \le y \le 20 \text{ cm} \end{cases}, \quad \text{(Eq 25)}$$

where the unit system is CGS. The ranges and characteristics of parameters in Eq 25 are listed in Table 1. Equation 25 can be used to predict the value of the SMD in the downstream region of spray based on the initial operating parameters for various atomized liquid. The application and validation of Eq 25 will be presented in Sect. 5.

5. Results and Discussion

5.1 Droplet Size and Its Distribution

Droplet mean size along the axial distance is the main concern in present study. As indicated in Sect. 4, the droplet diameter first decreases and then increases with the axial distance. In order to better understand the reason behind this trend, the benchmark case has been taken as an example to analyze the effects of particle secondary breakup and collision on the evolution of droplet mean size. As can be seen from Fig. 8, the droplet distortion and secondary breakup dominate at the nozzle exit due to the large velocity difference between the droplet and atomization gas, causing the drop size to rapidly decrease. While, at the downstream of the spray, the collision and coalescence play an important role due to a small velocity difference and larger drop densities, causing the drop diameter to gradually increase.

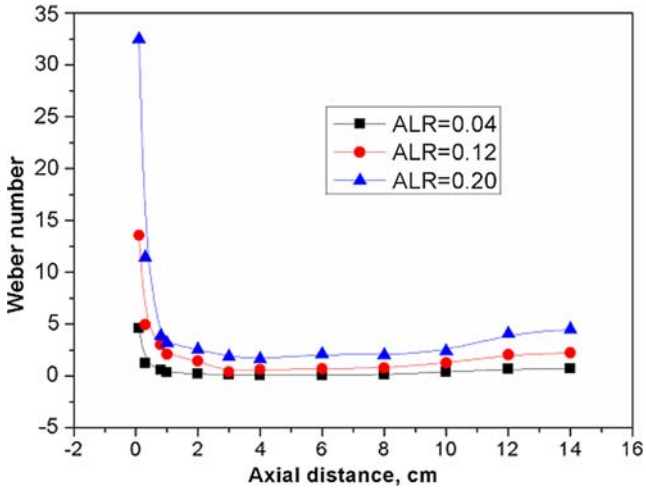

Fig. 10 Weber number along axial direction under different air-to-liquid mass flow ratio

In addition to the droplet mean diameter, the distribution of droplet size and number are also critical to the applications of atomization spray. Figure 9 shows the distributions of droplets' number and size on three cross-sectional planes located at the axial distance of 50, 100, and 150 mm, respectively. Results show that with the increase of the axial distance, the distribution of droplet locations becomes wider and the large droplets located closed to the spray core as a result of higher particle density and collision frequency. Moreover, due to the gravity effect, the center positions of droplets locations become slightly lower of the nozzle axis as the increase of axial distance.

In the applications of thermal spray, the Weber number of arriving material is of particular interest. The Weber number is defined as (Ref 26): $We = \rho_g |U|^2 d_d / \sigma_l$, where ρ_g is the gas density, U is the relative velocity of gas and drop, d_d is the droplet diameter, and σ_l is the liquid surface tension. Figure 10 shows the evolution of average Weber number along axial direction under different ALR ranging from 0.04 to 0.2, where the gas density is taken as the air density at standard conditions, which is 1.29×10^{-3} g/cm^3 σ_l is 46 g/s^2 according with the benchmark case. It can be observed that at the nozzle exit, the Weber number is much higher due to the large difference between the velocity of droplet and gas, causing the secondary breakup

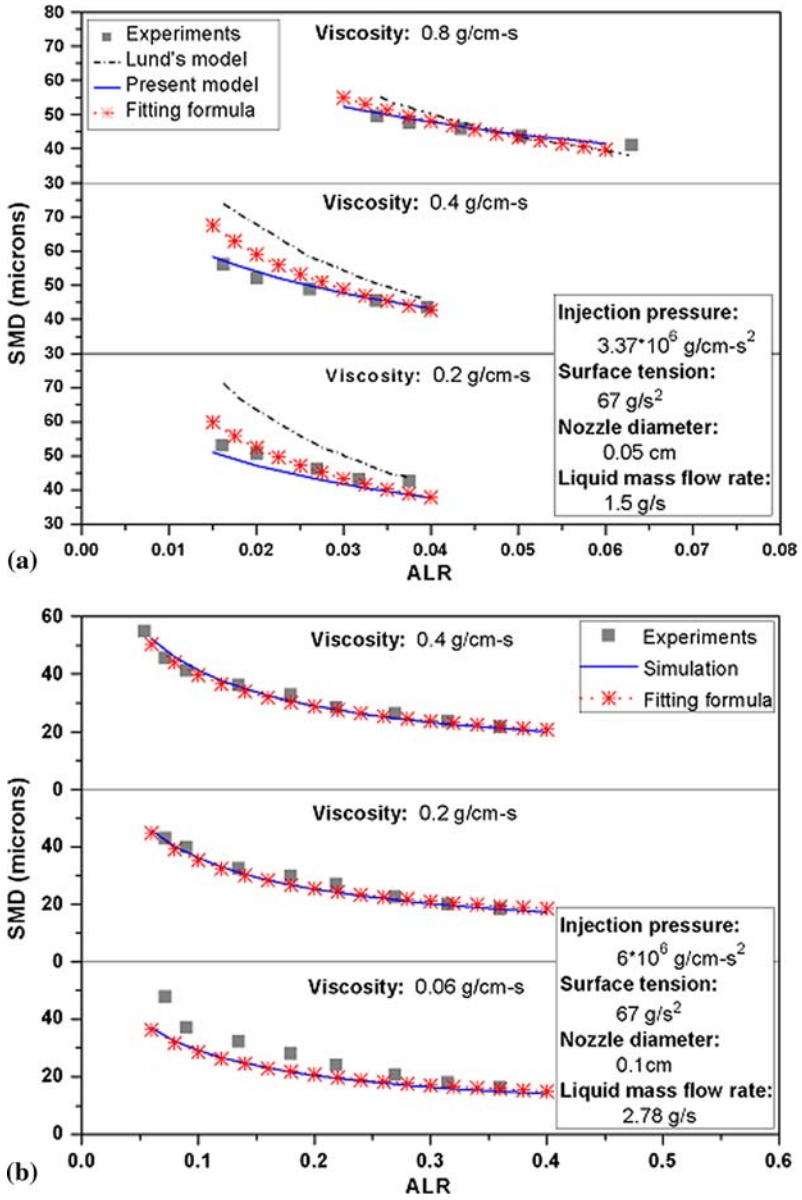

Fig. 11 Comparison of predicted SMD_0 from the fitting expression with experimental and numerical results for various viscosities. (a) Compared with Lund et al.'s model and experiments and (b) compared with Liu et al.'s experiments

of droplets; then with rapid decrease of droplet size and relative gas-drop velocity, the Weber number dramatically declines; while at the downstream of the spray, the Weber number slightly increases with the axial distance due to a gradual increase in the droplet size. Figure 10 also evidently indicated that as ALR increases, the Weber number increases as a result of higher relative gas-liquid velocity.

5.2 Validation of the Fitting Expression of SMD_0

To validate the primary breakup model and fitting expression of SMD_0, the results calculated from Eq 23 are compared with experimental data (Ref 9, 13) and numerical results for liquids with differing viscosity and surface tension.

Figure 11(a) indicates the fitting results agree well with the experimental data (Ref 9) and the numerical results for predictions of various viscosities (0.2–0.8 g/cm · s), in which the injection pressure is 3.37×10^6 g/cm · s^2, liquid surface tension is fixed as 67 g/s^2, nozzle exit diameter is 0.05 cm, liquid mass flow rate is 1.5 g/s and ALR changes from 0.015 to 0.06. Figure 11(a) also shows that the present model is better than that of Lund et al.'s (Ref 9) in these cases, since the present model improved Lund et al.'s model by considering the effect of relative velocity between the atomizing gas and liquid. Figure 11(b) compared the fitting results with simulation results and experimental data (Ref 13) for liquids of viscosity varying from 0.06 to 0.4 g/cm · s under operating conditions of $P_{in} = 6 \times 10^6$ g/cm · s^2, $D_{noz} = 0.1$ cm, $\dot{m} = 2.78$ g/s, $\sigma_l =$ 67 g/s^2, ALR = 0.05–0.4.

Figure 12 shows both the calculated results from fitting formula Eq 23 and simulations are in good agreement with experimental data (Ref 13) for the liquids with surface tension of 22-72 g/s^2 at $P_{in} = 4 \times 10^6$ g/cm · s^2, $\mu_l = 0.01$ g/cm · s, $D_{noz} = 0.1$ cm, $\dot{m} = 4.17$ g/s.

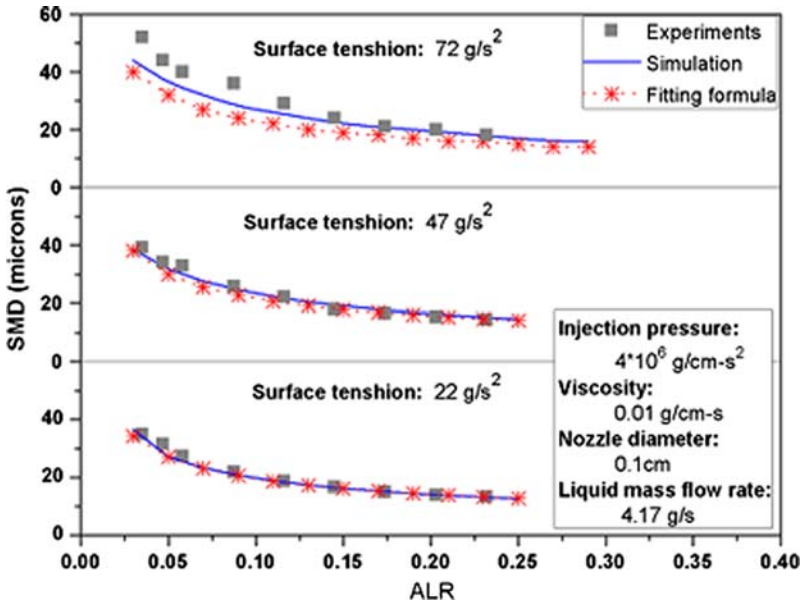

Fig. 12 Comparison of predicted SMD_0 from the fitting expression with experimental and numerical results for various surface tensions

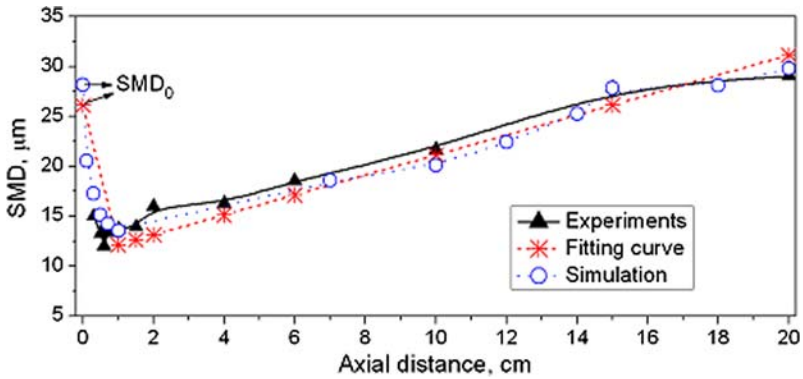

Fig. 13 Droplet Sauter mean diameter along the axial direction

Table 3 Comparison of predicted SMD from fitting expression with experimental results for various liquid under different operating conditions

	Operating conditions				Liquid physical properties		Droplet mean diameter SMD, μm	
Reference	Air-to-liquid mass ratio (ALR)	Injection pressure, P_{in}, 10^6 g/cm · s^2	Nozzle diameter, D_{noz}, cm	Axial distance, y, cm	Viscosity, μ_l, g/cm · s	Surface tension, σ_l, g/s^2	Exp.	Cal.
Liu et al. (Ref 11-13)	0.234	5	0.2	1	0.01	71.9	11.91	11.14
				1.5			12.77	11.61
				2			13.93	12.09
				4			14.37	14.00
				6			14.76	15.91
				10			19.04	19.72
				15			22.76	24.49
				20			25.14	29.26
	0.187			1			13.7	12.13
				1.5			13.93	12.63
				2			15.97	13.13
				4			16.3	15.13
				6			18.58	17.14
				10			21.71	21.14
				15			27.88	26.15
				20			29.03	31.15
Sutherland et. al. (Ref 10)	0.0076	2.9-7.8	0.038	15	0.8	30	64.2	68.55
	0.01						62.8	62.86
	0.0076				0.4		70.2	64.60
	0.01						68.5	59.31
	0.005				0.2		73.4	69.48
	0.0076						65.1	61.05
	0.01						63.3	56.12
Lund et al. (Ref 9)	0.016	3.37	0.05	15	0.2	67	55	70.10
	0.02						51.4	65.13
	0.027						47.2	59.03
	0.032						43.2	55.85
	0.0376						42.6	53.00
	0.026				0.4		49.8	63.98
	0.034						45.4	58.56
	0.04						43.4	55.51
	0.034				0.8		49.5	62.79
	0.038						47.4	60.50
	0.043						45.6	58.06
	0.05						43.7	55.23
	0.063						40.9	51.18
Petersen et al. (Ref 2)	0.128	11.72	0.06	15	0.25	45	30	30.91
	0.174						23.5	28.19
	0.225						20.3	26.11
	0.3						18.8	23.97
	0.08	5.52			0.03	44	35.3	30.44
	0.118						28.8	27.21
	0.158						24.6	25.03
	0.31						18.8	20.69
	0.54						16.2	17.73
	0.13	11.72					27.9	26.47
	0.19		0.06	15	0.03	44	22.8	23.75
	0.24						19.4	22.24
	0.32						16.3	20.51
	0.46						14.5	18.54
	0.132				0.12		27.6	28.82
	0.187						20.9	26.01
	0.245						18.8	24.04
	0.134				0.28	45	27.3	30.74
	0.187						21.7	27.81
	0.245						19.8	25.66
	0.16				1.32	46	40.5	33.21
	0.24						26.7	29.28
	0.32						22.3	26.80
	0.403						20.3	24.97
	0.55						17.9	22.72

Table 3 continued

Reference	Operating conditions: Air-to-liquid mass ratio (ALR)	Operating conditions: Injection pressure, P_{in}, 10^6 g/cm · s^2	Operating conditions: Nozzle diameter, D_{noz}, cm	Operating conditions: Axial distance, y, cm	Liquid physical properties: Viscosity, μ_l, g/cm · s	Liquid physical properties: Surface tension, σ_l, g/s^2	Droplet mean diameter SMD, μm: Exp.	Droplet mean diameter SMD, μm: Cal.
Nielsen et al. (Ref 3)	0.09	11.72	0.05	5	0.24	47	28.3	23.15
	0.2						19.2	17.53
	0.3						16.1	15.25
	0.05				1.82		44.7	36.63
	0.087						38.2	29.98
	0.38						23.3	17.73

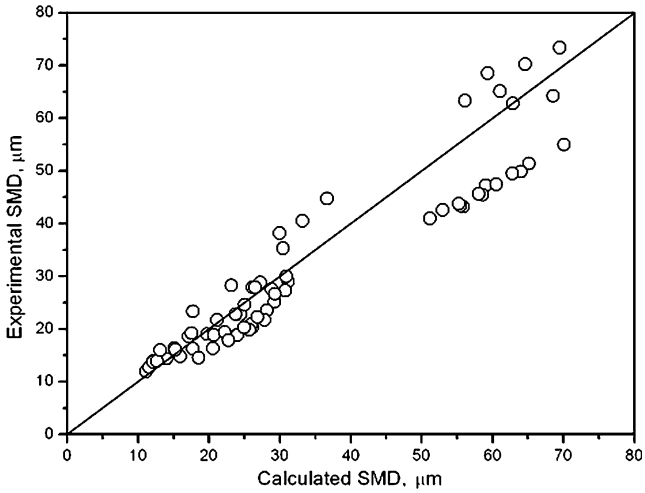

Fig. 14 Experimental Sauter mean diameter vs. calculated Sauter mean diameter

5.3 Validation of the Fitting Expression of SMD

Figure 13 compares the fitting results of SMD along the axial direction with the experimental (Ref 12) and numerical data at $P_{in} = 5 \times 10^6$ g/cm · s^2, $\mu_l = 0.01$ g/cm · s, $\sigma_l = 71.9$ g/s^2, $D_{noz} = 0.2$ cm, $\dot{m} = 2.5$ g/s. The fitting curve used in Fig. 13 is expressed as:

$$\text{SMD } (\mu\text{m}) = \begin{cases} \text{SMD}_0 = 26.11 & y \to 0 \\ (k + kk + \text{SMD}_0) \times y + \text{SMD}_0 = -13.9807 \times y + 26.11 & 0 < y < 1 \text{ cm} \\ k \times y + kk = 1.0013 \times y + 11.128 & 1 \text{ cm} \le y \le 20 \text{ cm} \end{cases}, \quad \text{(Eq 26)}$$

where SMD_0 and k, kk are calculated from Eq 23 and 24. As shown in Fig. 13, the fitting results agree well with the experiments and numerical results in the downstream region of spray. It also can be seen that the fitting results deviate from the experimental and numerical results obviously when y is less than 1 cm. The reason is that the effects of injection pressure, atomizer diameter and liquid mass flow rate on the secondary atomization are neglected in the derivation of Eq 25. However, it is reasonable to use Eq 24 to calculate the droplet mean diameter at the downstream spray beyond 1 cm from the nozzle orifice for most engineering applications.

Table 3 provides abundant experimental results (Ref 2, 3, 9-13) to compare with the predicted SMD under various conditions. The ranges of the operating conditions and liquid physical properties presented in Table 3 are ALR = 0.005–0.55, $P_{in} = 2.9$–11.72×10^6 g/cm · s^2, $D_{noz} = 0.038$–0.2 cm, $y = 1$–20 cm, $\mu_l = 0.01$–1.82 g/cm · s, $\sigma_l = 30$–71.9 g/s^2. Figure 14 indicates that the results calculated from the fitting formula (Eq 25) agree with the experimental data in Table 3 to within 30%.

6. Conclusion

The outflow of a typical effervescent atomization spray is simulated numerically by a comprehensive numerical model based on the Navier-Stokes equation and the particle tracking method. The gas flow field is assumed to be axisymmetric and the dispersed phase droplet is modeled as Lagrangian entities. Droplet mean size, one of the most important spray characteristics, was calculated extensively under different operating conditions and liquid physical properties. The evolution of Weber number and the distribution of droplet size and number along axial direction have also been discussed. The curve fitting technique is used to dispose the extensive numerical results on the purpose of deducing a formula to quantize the effects of important operating conditions and liquid properties on droplet mean diameter. After abundant validations, the deduced formula (Eq 25) can be used to predict droplet Sauter mean diameter at the downstream region in the

axisymmetric effervescent atomization spray for various Newtonian liquid conveniently and effectively.

Acknowledgments

This work was supported by the Major Program of the National Natural Science Foundation of China with Grant No 10632070 and the National Natural Science Foundation of China with Grant No. 10602052.

References

1. S. Tonini, M. Gavaises, and A. Theodorakakos, The Role of Droplet Fragmentation in High-Pressure Evaporating Diesel Sprays, *Int. J. Therm. Sci.*, 2009, **48**, p 554-572
2. F.J. Petersen, O. Worts, T. Schafer, and P.E. Sojka, Effervescent Atomization of Aqueous Polymer Solution and Dispersions, *Pharm. Dev. Technol.*, 2001, **6**, p 201-210
3. A.F. Nielsen, P. Bertelsen, H.G. Kristensen, J. Kristensen, and L. Hovgaard, Investigation and Comparison of Performance of Effervescent and Standard Pneumatic Atomizer Intended for Soluble Aqueous Coating, *Pharm. Dev. Technol.*, 2006, **11**, p 243-253
4. J.O. Berghaus, J.G. Legoux, C. Moreau, F. Tarasi, and T. Chraska, Mechanical and Thermal Transport Properties of Suspension Thermal-Sprayed Alumina-Zirconia Composite Coatings, *J. Therm. Spray Technol.*, 2008, **17**, p 91-104
5. S.A. Esfarjani and A. Dolatabadi, A 3D Simulation of Two-Phase Flow in an Effervescent Atomizer for Suspension Plasma Spray, *Surf. Coat. Technol.*, 2009, **203**, p 2074-2080
6. L.D. Xie, D.Y. Chen, E.H. Jordan, A. Ozturk, F. Wu, X.Q. Ma, B.M. Cetegen, and M. Gell, Formation of Vertical Cracks in Solution-Precursor Plasma-Sprayed Thermal Barrier Coatings, *Surf. Coat. Technol.*, 2006, **201**, p 1058-1064
7. S.D. Sovani, P.E. Sojka, and A.H. Lefebvre, Effervescent Atomization, *Prog. Energy Combust. Sci.*, 2001, **27**, p 483-521
8. A.H. Lefebvre, A Novel Method of Atomization with Potential Gas Turbine Application, *Ind. Defence Sci. J.*, 1988, **38**, p 353-362
9. M.T. Lund, P.E. Sojka, A.H. Lefebvre, and P.G. Gosselin, Effervescent Atomization at Low Mass Flow Rates, Part 1: The Influence of Surface Tension, *Atomization Sprays*, 1993, p 77-89
10. J.J. Sutherland, P.E. Sojka, and M.W. Plesniak, Ligament-Controlled Effervescent Atomization, *Atomization Sprays,* 1997, **7**, p 383-406
11. L.S. Liu, ''Experimental and Theoretical Investigation on the Characteristics and Two-Phase Spray Flow Field of Effervescent Atomizers,'' Ph.D. Thesis, Tianjing University, China, 2001
12. L.S. Liu, M.L. Fu, J.X. Wu et al., The Distribution of SMD Downstream the Discharge Orifices of Effervescent Atomizers, *J. Eng. Thermophys.*, 2001, **22**, p 653-656 (in Chinese)
13. L.S. Liu, J.X. Wu, Z.X. Han, and L.M. Fu, Studies of Effervescent Atomization at Different Physical Properties of Spray Fluid, *J. Therm. Sci. Technol.*, 2002, **2**, p 128-132 (in Chinese)
14. H.E. Buckner and P.E. Sojka, Effervescent Atomization of High Viscosity Fluids, Part 2: Non-Newtonian Liquids, *Atomization Sprays*, 1993, **3**, p 157-170
15. H.B. Xiong, J.Z. Lin, and Z.F. Zhu, Three-Dimensional Simulation of Effervescent Atomization Spray, *Atomization Sprays*, 2009, **19**, p 1-16
16. J.Z. Lin, L.J. Qian, and H.B. Xiong, Relationship Between Deposition Properties and Operating Parameters for Droplet onto Surface in the Atomization Impinging Spray, *Powder Technol.*, 2009, **191**, p 340-348
17. M.T. Lund and C.Q. Jian, The Influence of Atomizing Gas Molecular Weight on Low Mass Flow-Rate Effervescent Atomization Performance, *J. Fluids Eng.*, 1998, **120**, p 750-754
18. M. Ishii, One Dimensional Drift-Flux Mode and Constitutive Equations for Relative Motion between Phases in Various Two-phase Flow Regimes, Argonne National Laboratory Report, 1977, p 47-77
19. N.E. Todreas and M.S. Kazimi, *Nuclear Systems I: Thermal Hydraulic Fundamentals*, Hemisphere, New York, 1989
20. P.K. Senecal, D.P. Schmidt, I. Nouar, C.J. Rutland, R.D. Reitz, and M.L. Corradini, Modeling High-Speed Viscous Liquid Sheet Atomization, *Int. J. Multiphase Flow*, 1999, **25**, p 1073-1097
21. F.X. Tanner, Development and Validation of a Cascade Atomization and Drop Breakup Model for High-Velocity Dense Sprays, *Atomization Sprays*, 2004, **14**, p 211-242
22. R.D. Reitz, Modeling Atomization Processes in High-Pressure Vaporizing Sprays, *Atomization Spray Technol.*, 1987, **3**, p 309-337
23. P.J. O'Rourke and A.A. Amsden, The TAB Method for Numerical Calculation of Spray Droplet Breakup, SAE Paper, 872089, 1987
24. P. Rosin and E. Rammler, The Laws Governing the Fineness of Powdered Coal, *J. Inst. Fuel*, 1933, **7**, p 29-36
25. J.D. Whitlow and A.H. Lefebvre, Effervescent Atomizer Operation and Spray Characteristics, *Atomization Sprays*, 1993, **3**, p 137-156
26. J. Fazilleau, C. Delbos, V. Rat, J.F. Coudert, P. Fauchais, and B. Pateyron, Phenomena Involved in Suspension Plasma Spraying Part 1: Suspension Injection and Behavior, *Plasma Chem. Plasma Process.*, 2006, **26**, p 371-391